Chemical Engineering Journal 156 (2010) 471–478

Contents lists available at ScienceDirect

Chemical Engineering Journal

journal homepage: www.elsevier.com/locate/cej

Stability and thermal conductivity of nanofluids of tin dioxide synthesized via microwave-induced combustion route

Sajjad Habibzadeh[a,b,*], Amin Kazemi-Beydokhti[a], Abbas Ali Khodadadi[a], Yadollah Mortazavi[a], Sasha Omanovic[b], Mojtaba Shariat-Niassar[a]

[a] School of Chemical Engineering, University College of Engineering, University of Tehran, Tehran, Iran
[b] Department of Chemical Engineering, McGill University, 3610 University Street, Montreal, Que., Canada H3A 2B2

ARTICLE INFO

Article history:
Received 26 June 2009
Received in revised form 26 October 2009
Accepted 4 November 2009

Keywords:
Tin oxide
Combustion synthesis
Nanofluid
Colloidal stability
Thermal conductivity

ABSTRACT

SnO_2 nanofluids were prepared by dispersing tin dioxide nanoparticles in deionized (DI) water as a base fluid. 4–5 nm tin dioxide crystals were synthesized via chloride solution combustion synthesis (CSCS) using $SnCl_4$ and sorbitol as a novel precursor and the fuel, respectively. Ammonium nitrate was also used as the combustion aid. The molar ratio of sorbitol plus ammonium nitrate to $SnCl_4$ was set at unity; whereas, the molar ratio of sorbitol-to-ammonium nitrate divided by that of stoichiometric value (Φ) was varied in the range of 0.5–1.4 in order to find the optimum values of specific surface area for the CSCS technique. Transition electron microscopy (TEM), scanning electron microscopy (SEM), powder X-ray diffraction (XRD), and Brunauer–Emmet–Teller (BET) techniques were employed for the characterization of the nanoparticles. Since SnO_2 nanoparticles form clusters within fluids, the fluids were ultrasonicated to improve the dispersion and stability of the nanoparticles. The colloidal stability of the SnO_2 nanofluids was quantitatively characterized by UV–vis spectrophotometric measurements. The results of the UV–vis experiments indicate higher dispersion together with enhanced stability for the nanofluid prepared by SnO_2 nanoparticles synthesized at $\Phi = 1.0$. After 500 h sedimentation time, the relative concentration of the nanofluid with the highest stability is remained at around 77% of the initial concentration of the fluid.

A transient hot-wire apparatus was used to measure the thermal conductivities of the nanofluids. In addition, the effects of pH and temperature on the thermal conductivity were also investigated. At 353 K, for the nanofluid prepared by SnO_2 nanoparticles synthesized at $\Phi = 1.0$ at a weight fraction of 0.024%, thermal conductivity is enhanced up to about 8.7%, with an optimal pH = 8.

1. Introduction

With an ever-increasing thermal load due to trends toward smaller microelectronic devices, greater power output for engines, and brighter beams for optical devices, cooling of such devices and related systems is a crucial issue in high-tech industries such as microelectronics, transportation and advanced nuclear systems. The conventional approach for increasing cooling rates is the use of extended surfaces such as fins and microchannels. However, current designs have already stretched this approach to its limits. Therefore, there is an urgent need for new and innovative concepts to achieve ultra-high-performance cooling. It has been recognized for a long time that the fluid suspensions of solid particles provide useful advantages in industrial fluid systems, including heat transfer fluids, magnetic fluids, and lubricant fluids [1,2]. The key idea is to exploit the very high thermal conductivities of solid particles, which can be hundreds or even thousands of times greater than those of conventional heat transfer fluids such as water and ethylene glycol.

Nanofluids, i.e. fluid suspensions of nanometer-sized solid particles and fibers, have been firstly proposed by Choi [3] as a route for surpassing the performance of common heat transfer liquids [4]. The much larger relative surface area of nanoparticles, compared to those of micro-scale particles, not only significantly improves heat transfer capabilities, but also increases the stability of the nanofluid suspensions. The enhancement of thermal-transport properties of such "nanofluids" is even greater than that of suspensions of coarse-grained materials [5–7]. Keblinski et al. [8] listed four possible explanations for the cause of an anomalous increase of thermal conductivity: Brownian motion of the nanoparticles, molecular-level layering of the liquid at the liquid/particle interface, the nature of heat transport in the nanoparticles, and the effects of nanoparticles clustering.

Although such suspensions do indeed exhibit the appropriate augmentation in thermal conductivity, they suffer from stability

* Corresponding author at: Department of Chemical Engineering, McGill University, 3610 University Street, Montreal, Que., Canada H3A 2B2.
E-mail address: sajjad.habibzadeh@mail.mcgill.ca (S. Habibzadeh).

1385-8947/$ – see front matter © 2009 Elsevier B.V. All rights reserved.
doi:10.1016/j.cej.2009.11.007

and rheological problems. Especially, the particles tend to swiftly settle out of suspensions thereby cause severe clogging, particularly, in mini- and microchannels. Contrary to the milli- and microsized particle slurries explored in the past, nanoparticles are relatively close in size to the molecules of the base fluid, and thus can realize very stable suspensions with little gravitational settling over long periods of time [9]. Generally, there are two common techniques for the preparation of nanofluids: the single-step [10] and the two-step method [11]. As compared to the single-step method, the two-step technique shows better results for oxide nanoparticles, while it is lesser successful for metallic particles.

Many methods have been developed to synthesize SnO_2 nanoparticles [12–16]. Since the two-step method strongly depends upon the method of synthesis of nanoparticles, we utilize the SnO_2 nanoparticles synthesized through a novel technique named chloride solution combustion synthesis (CSCS) [17]. Solution combustion synthesis (SCS) which have been developed over 20 years is a simple and single-step method to synthesize ultrafine powders of metal oxides. SCS method relies on a self-sustained combustion reaction between a fuel and an oxidizer. SCS typically uses a metal precursor in the nitrate form. Reaction between the fuel and oxygen containing species, formed during the decomposition of the nitrite species, provides high temperature which facilitates rapid interactions [18–25]. In addition, according to the literature, microwave has been used for fast and homogeneous heating of the combustion synthesis solutions [17].

Since long-term stability is a crucial characteristic of nanofluids, study of the colloidal stability of the nanofluids is of great importance. Nanofluids dispersing carbon nanotubes, copper, aluminum and their oxide, titania [26–32] nanoparticles have been widely investigated by many researchers. However, tin dioxide, which has excellent chemical and physical stability, is not widely used although it is a cheap and commercially available mineral product. In this work, for the first time, SnO_2 nanofluids are prepared by dispersion of tin dioxide nanoparticles in DI water as the base fluid. A microwave-induced combustion synthesis method using tin chloride precursor along with the ammonium nitrate salt as a combustion aid and sorbitol as the fuel, is used to prepare SnO_2 nanoparticles [17,33–34]. Three fuel-to-ammonium nitrate molar ratios are used for synthesis of different tin dioxide nanoparticles in order to prepare nanofluids with various stabilities. The ultrasonication technique is employed to disperse the nanoparticles properly and form nanofluids with high stabilities.

The surface chemical behavior changes the suspension stability through surface charge states and thereby surface potential. Therefore, in the present study we have changed pH of the suspension systematically to control surface potential that can be reflected by zeta potential. The effects of the pH value of the aqueous suspension, the temperature of nanofluids and the weight fraction of the dispersed SnO_2 nanoparticles on the thermal conductivity have been studied as well.

2. Experimental

2.1. Preparation of SnO_2 nanoparticles

For preparation of SnO_2 by the chloride solution combustion synthesis (CSCS) method, extra pure $SnCl_4$, sorbitol and analytical grade ammonium nitrate (all from Merck) were used as starting materials. Proper amounts of NH_4NO_3 and sorbitol were dissolved in a $SnCl_4$ aqueous solution and the sample was heated at ~100 °C and stirred for 10 min to remove excess water. The viscous transparent aqueous solution in a crucible was introduced into a microwave oven with 850 W microwave sources. The sample was brought to the combustion temperature by microwave-induced homogeneous heating. Spontaneous and self-propagating decomposition and/or combustion of the sample produce a large amount of heat and gas. The whole combustion process takes about 3 min. In order to eliminate possible carbonaceous residues and to stabilize the microstructure of SnO_2 powders, without excessive grains growth, the as synthesized powder was subsequently calcined at 400 °C in air for 3 h. Powders were then centrifuged and washed with distilled water in order to eliminate chloride ions and then dried at room temperature.

The concentration of sorbitol for the stoichiometric reaction was calculated using the propellant criterion as described by Jain et al. [35]. Considering the following valences for the elements: C = +4, H = +1, O = −2, N = 0, the oxidizing valence of NH_4NO_3 is −2 and the reducing valence of sorbitol is +26, so the stoichiometric molar ratio of NH_4NO_3/sorbitol is 13. The molar ratio of fuel-to-oxidant divided by that of stoichiometric value (Φ) and the ratio of fuel plus oxidant to $SnCl_4$ (Ψ) are also varied.

$$SnCl_4 + NH_4NO_3 + \frac{2}{26}\Phi C_6H_{14}O_6 + \frac{1}{2}(\Phi - 1)O_2 \rightarrow SnO_2 + \frac{12}{26}\Phi CO_2 + 4HCl + N_2 + \frac{14}{26}\Phi H_2O \quad (1)$$

In the equation mentioned above, $\Phi = 1$ means that the initial mixture does not require atmospheric oxygen for complete oxidation of fuel, whereas $\Phi > 1$ (<1) implies fuel rich (lean) conditions.

2.2. Characterization of SnO_2 powders

The crystalline structures and approximate sizes of the SnO_2 samples were determined by X-ray powder diffraction (XRD) with a Philips-X'pert diffractometer using Cu Kα radiation (λ = 1.54056 Å). Crystal size of the SnO_2 powders was determined by applying Scherrer formula on (1 1 0) diffraction peak. The BET surface area measurement was also carried out by nitrogen adsorption after degassing of the samples at 300 °C for 2 h, using a Quantachrome CHEMBET-3000 apparatus. Transition electron microscopy (TEM) and scanning electron microscopy (SEM) of as synthesized SnO_2 samples were done using Philips CM 200 and CamScan MV 2300, respectively.

2.3. Preparation of SnO_2 nanofluids

For the sake of simplicity, SN0.5, SN1.0 and SN1.4 stand for the SnO_2 nanoparticles synthesized at $\Phi = 0.5$, 1.0 and 1.4, respectively. SN0.5, SN1.0 and SN1.4 nanofluids were prepared via a two-step procedure by dispersing the nanoparticles in DI water as the base fluid. Since no stabilizing agents, i.e. surfactants were added in the preparation of nanofluids, it is expected that the nanoparticles form clusters in nanofluid samples. In order to improve the dispersion of particles in fluid samples, the nanofluids were ultrasonicated for 2 h using the ultrasonic processor (Bandelin Sonoplus-HD3200 model, power – 200 W, frequency – 20 kHz). Then zeta potential and particle size were measured by a Malvern Nano-ZS (Malvern Instrument Inc., London, UK). The pH was controlled using hydrochloric acid (HCl) and sodium hydroxide (NaOH) of analytical grade.

Ultrasonication is an external mechanical energy that helps the particles to overcome the attractive van der Waals force at contact. Even though the sonication cannot break nanoparticles individually, the cluster of nanoparticles breaks into smaller clusters resulting in the smaller clusters with higher stability.

2.4. Measurement of the thermal conductivity of nanofluids

Thermal conductivity measurement is preformed with a transient hot-wire technique, which is known as an accurate method for

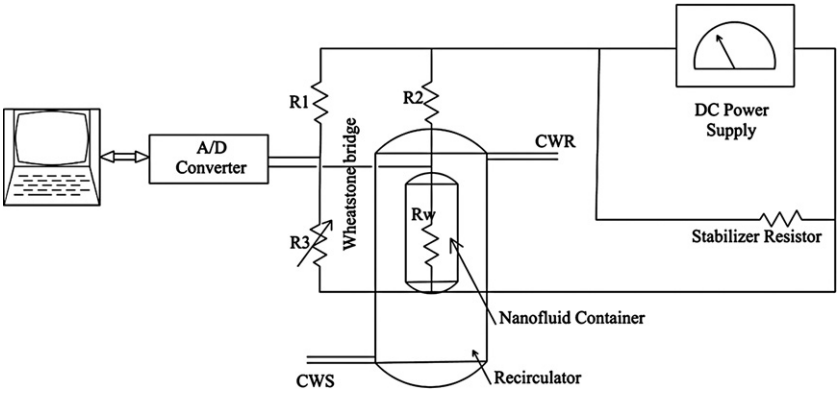

Fig. 1. Schematic diagram of a transient hot-wire apparatus.

determining thermal conductivities of fluids. A schematic diagram of the system used in this study is shown in Fig. 1. Pure platinum wire with a diameter of 0.5 mm and length of 3 cm was used as a hot wire. The wire is coated with Teflon to remove the effect of static charge and electrical conductance of particles. Measured thermal conductivities of the nanofluid are normalized to those of the base fluids. The thermal conductivity of the liquid is determined from the temperature change of the wire and the heat generation.

In this apparatus R4 is a 20 Ω dummy resistor used to stabilize the DC power supply. In the Wheatstone bridge, R_1 is a 1 kΩ potentiometer, R_2 is a 1 kΩ resistor, and R_3 is a 19 Ω resistor and R_w is the resistance of the platinum wire. In order to minimize temperature fluctuations, the hot-wire cell was placed in a thermostatic bath at the control temperature for which the thermal conductivity measurements were performed. The energy equation of this system is written from Fourier's law as:

$$\frac{1}{\alpha}\frac{\partial T}{\partial t} = \frac{1}{r}\frac{\partial}{\partial r}\left(r\frac{\partial T}{\partial r}\right) \tag{2}$$

And the thermal conductivity k is calculated from following equation [36]:

$$q = \frac{I^2 R}{l} \tag{3}$$

$$k = \frac{q}{4\pi(T_2 - T_1)}\ln\left(\frac{t_2}{t_1}\right) \tag{4}$$

where R is the resistance of the wire, l is the wire length, and I is the electric current. α is the thermal diffusivity, T_1 and T_2 are the temperatures at time t_1 and t_2, and q is the applied electrical power. From the temperature coefficient of the platinum wire's resistance, the temperature rise can be determined by the change in its electrical resistance with time. Using distilled water and ethylene glycol as standard liquids of known thermo-physical properties, the measurements of the hot wire are calibrated. The temperatures are recorded every 0.01 s during 1 s to be used in Eq. (4) to calculate the thermal conductivity.

3. Results and discussion

The X-ray diffraction patterns of the samples prepared by chloride solution combustion synthesis (CSCS) method and calcined at 400 °C for 3 h at lean, stoichiometric, and rich fuel conditions are illustrated in Fig. 2. The characteristic peaks of the cassiterite phase (JCPDS No. 41-1445) at 26.6, 33.8 and 51.8 two theta degrees and associated $h\,k\,l$ Miller indexes of (1 1), (1 0 1) and (2 1 1), respectively, have been identified in the XRD patterns. The Scherrer's crystallite sizes obtained from the XRD patterns are summarized in Table 1. The average crystallite size decreases as Φ increases from 0.5 to 1.0. The difference between crystallite and particle sizes sharply decreases at $\Phi = 1.0$ to a minimum of 0.7 then slightly increases as Φ increases to 1.4. This may indicate the lowest degree of aggregation, which leads to the highest surface area, for the stoichiometric fuel-to-oxidant ratio ($\Phi = 1.0$).

Table 1
XRD crystallite sizes estimated from Scherrer's equation (d_{XRD}), BET surface areas, average particle sizes estimated from BET data (d_{BET}), and d_{BET}/d_{XRD} as an indication of degree of nanoparticles aggregation.

Sample	Crystallite sizes (d_{XRD}, nm)	BET surface area ($m^2\,g^{-1}$)	Particle size (d_{BET}, nm)	d_{BET}/d_{XRD}
SN0.5	5.3	85.6	10.0	1.89
SN1.0	4.3	171.6	5.0	1.08
SN1.4	4.3	126.8	6.8	1.58

Scherrer crystallite sizes, BET surface areas and estimated particle sizes of the SnO_2 samples synthesized at $\Psi = 1.0$ and various Φ's are listed in Table 1. Assuming spherical loose particles, the BET average particle sizes (d_{BET}) are estimated by equation $d = (6000/S_{BET} \times \rho)$, where S_{BET} is BET surface area (m^2/g) and ρ is skeletal density (g/cm^3). The ratio of the size of particles to that of crystallites, i.e. d_{BET}/d_{XRD}, which can be considered as a good representation of aggregation of the nanoparticles is also presented in Table 1.

SEM micrographs of as synthesized samples prepared at $\Phi = 0.5$, 1.0 and 1.4 are presented in Fig. 3. The aggregation ratios of the samples (see Table 1) are confirmed by the SEM micrographs. Another remarkable observation is the appearance of micron-size pores in the samples. These pores are shaped by the expansion of large

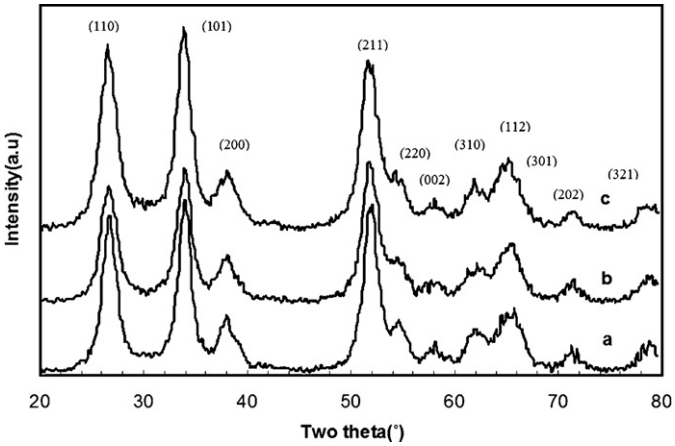

Fig. 2. XRD patterns of SnO_2 at various fuel-to-oxidant ratios: (a) $\Phi = 0.5$, $\Psi = 1.0$; (b) $\Phi = 1.4$, $\Psi = 1.0$; (c) $\Phi = 1.0$, $\Psi = 1.0$.

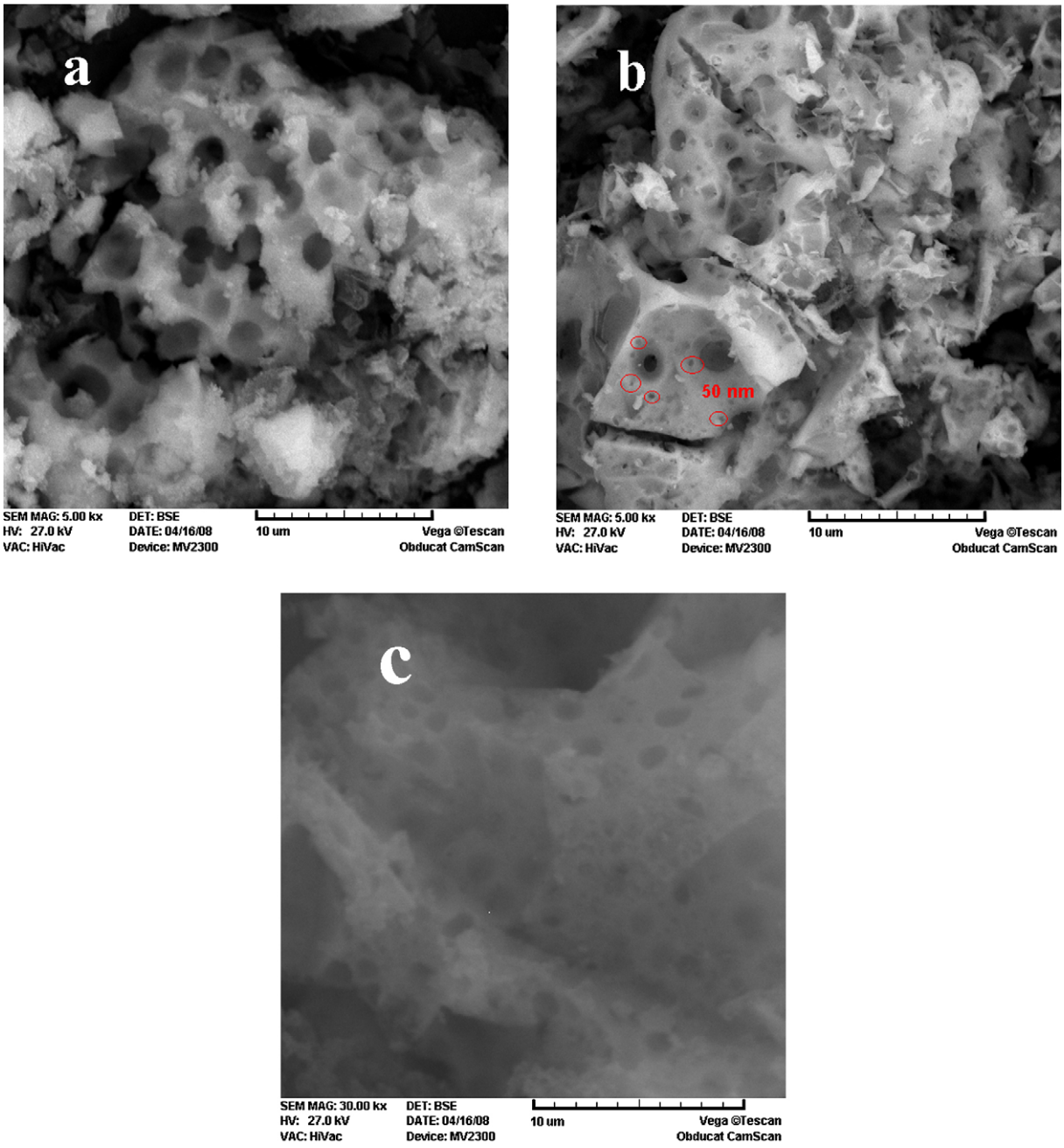

Fig. 3. SEM micrograph of SnO_2 prepared by CSCS (a) $\Phi = 0.5$, $\Psi = 1.0$; (b) Φ, $\Psi = 1.0$ and (c) $\Phi = 1.4$, $\Psi = 1.0$.

amounts of gas bubbles produced during the combustion. The bubbles pass through the synthesized sample resulting in micro-scale holes in the samples, as observed in the SEM micrographs. Fig. 3b shows small pores of about 50 nm size in SN1.0 sample.

The transition electron micrograph (TEM) of SnO_2 nanoparticles at fuel-to-oxidant 0.5 and 1.0 synthesized through chloride solution combustion synthesis are shown in Fig. 4. It is seen that the size of agglomeration at SN0.5 is larger than that of SN1.0.

Fig. 5 illustrates the particle size distributions of SN0.5 and SN1.0 nano-suspensions. The discrepancies in the particle size characteristics between two samples are evident. It is shown that the average particle sizes of SN1.0 and SN0.5 are 69 and 152 nm, respectively.

Recently, a new method which can be used to assess the suspension concentration of nanofluids with increasing the sedimentation time has been reported in the literature [37]. The stability of nanofluids is estimated by a UV–vis scanning spectrophotometer (SpectroFlex 6600).

Fig. 6 illustrates that the peak absorbance of SN0.5 and SN1.0 in DI water-based suspensions appear at 292 and 299 nm, respectively. The absorbance of SN0.5, SN1.0 and SN1.4 in DI water suspensions decreases with increasing sedimentation time. A linear calibration curve, as shown in Fig. 7, was constructed at wavelengths of 287, 292 and 299 nm for SN1.4, SN0.5 and SN1.0 nanofluids, respectively. The calibration curves were developed in the range of 0.01–0.025 wt% of the SnO_2 nanoparticles in the base fluid. The concentration of the supernatant particles in nanofluids was determined by fitting the absorbance to the calibration curve.

Fig. 8 shows the colloidal stability of the prepared nanofluids according to the results of UV–vis tests and based on initial concentration of the fluids, i.e. $C_0 = 0.024$ wt%. The trend of supernatant

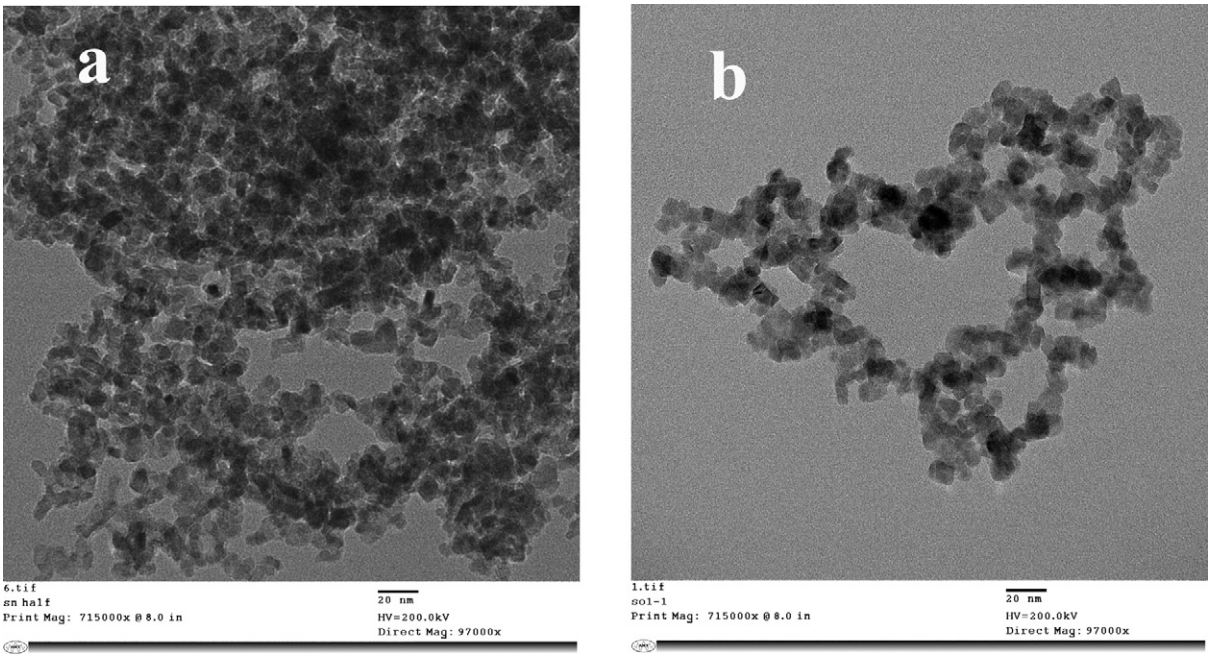

Fig. 4. Transition electron micrograph of (a) SN0.5 and (b) SN1.0.

particle concentration (C) in the base fluid as a function of the sedimentation time is always downward. In addition, the stability of nanofluids is completely dependent upon the parameters of the synthesis method, so that the nanofluid prepared by nanoparticles synthesized at $\Phi = 1.0$ is very stable, while a poor stability is observed for that prepared by SN1.4. It should be noted that after 500 h, relative concentration of SN1.0 nanofluid is remained to about 77% compared to initial concentration (C_0). It would be of interest to consider that the aggregation ratio (Table 1) of SN1.0, i.e. 1.08 is smaller than that of other samples, which is inline with the stability results. Furthermore, the SN0.5 nanoparticles have higher aggregation ratio compared to the SN1.4 sample (see Table 1); nevertheless, the nanofluid of SN0.5 nanoparticles is more stable than that of SN1.4. It can be ascribed to the nature of agglomeration which may be different in the samples. In other words, hard agglomeration of SN1.4 nanofluid is responsible for its difficult dispersion, resulting in lower stability of SN1.4 nanofluid.

Figs. 9 and 10 show the zeta potential and the thermal conductivity enhancement for SN1.0 (0.024 wt%) suspensions as a function of pH. The overall behavior of the particle–water interaction depends upon the properties of the particle surface. At the isoelectric point (IEP), the repulsive forces among SnO_2 nanoparticles are zero and nanoparticles will coagulate together under this pH value. Therefore, when the pH value is equal to or close to the IEP in the minimum surface charge state, SnO_2 nanoparticles suspension is unstable. The hydration forces among particles increase with the increasing difference of the pH value of a suspension from the IEP, which results in the enhanced mobility of nanoparticles in the suspension [32]. The microscopic motions of the particles cause microconvection that enhances the heat transport process. It is also observed as the pH goes away from the IEP, the surface

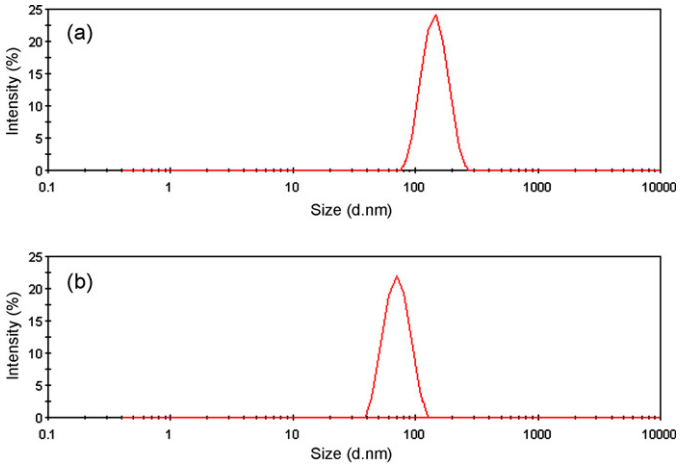

Fig. 5. Particle size distribution of (a) SN0.5 and (b) SN1.0.

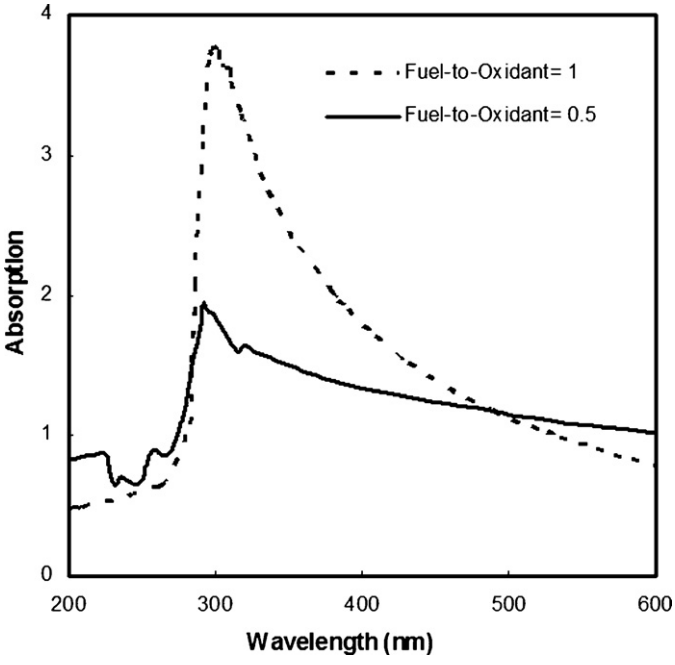

Fig. 6. UV–vis spectrum of SnO_2 nanoparticles in DI water.

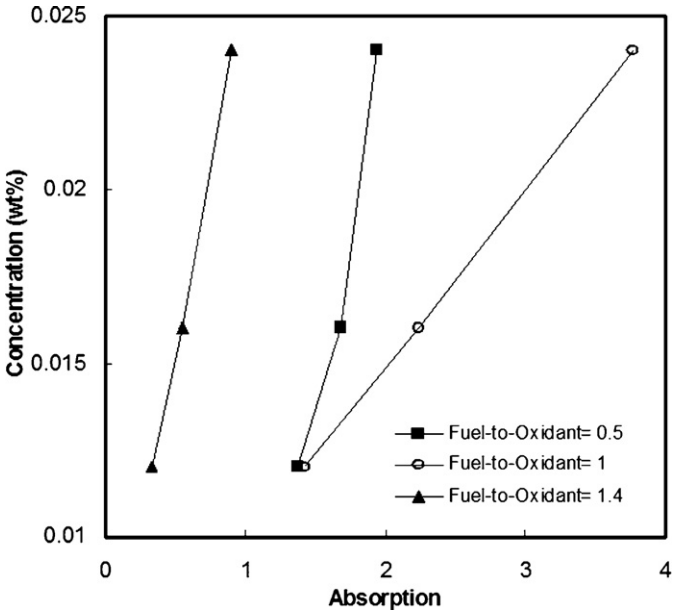

Fig. 7. Relationship between light absorption and concentration of SnO_2 in DI water at maximum wavelengths.

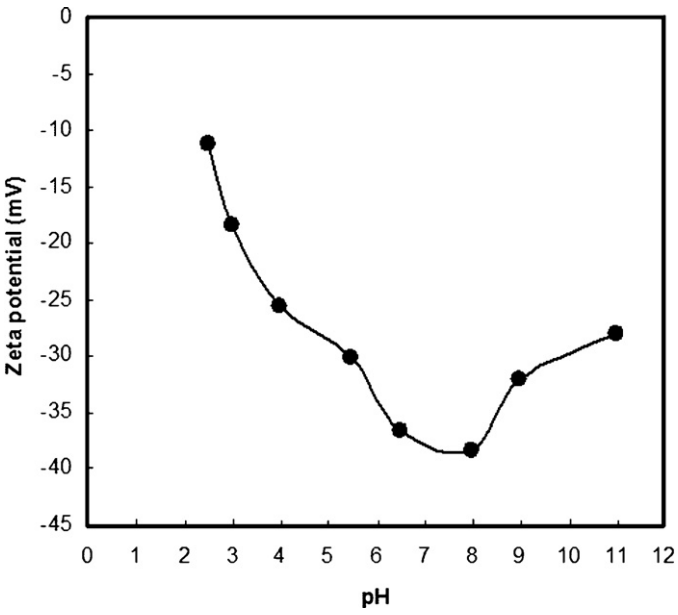

Fig. 9. . Effect of pH on zeta potential of SN1.0 (0.024 wt%) nanofluid.

charge increases because of strongly repulsive double-layer (interfacial) force according to the DLVO theory [38,39] generated by the very high surface charges, leading to an increase in the zeta potential on the SnO_2 powder surface [40]. As can be seen the thermal conductivity increases with increase of pH value from 3.0 to 8.0. One can observe that there are more surface charges at around pH 8.0, at which the dispersion behavior is better and thereby the thermal conductivity is higher. Under strong acidic conditions or strong basic conditions, thermal conductivity ratios have a tendency to decrease. It may be attributed to the decreasing of the absolute value of zeta potentials in this range of pH, because under the both conditions, more H^+ ions and OH^- ions are needed to adjust pH values.

Thermal conductivity enhancement of nanoparticles synthesized at various fuel-to-oxidant ratio suspensions as a function of solid weight fraction is depicted in Fig. 11. The thermal conductivities of nanofluids are enhanced with increase of the SnO_2 nanoparticles weight fraction. The maximum thermal conductivity enhancement of 7.0% is observed at the 0.024 wt% suspension.

The effect of temperature on the enhancement of thermal conductivity of nanofluids is also investigated by measuring the thermal conductivity of nanofluids for different temperatures ranging from 293 to 353 K. As observed in Fig. 12 the thermal conductivity of SN1.0 nanofluid increases by about 8.7% at 353 K. The thermal conductivity of different nanofluids increases significantly with the fluid temperature. This is because the high fluid temperature intensifies the Brownian motion of nanoparticles and also decreases the viscosity of the base fluid. With an intensified Brownian motion, the contribution of microconvection in heat transport increases which results in increased enhancement of the thermal conductivity of nanofluids.

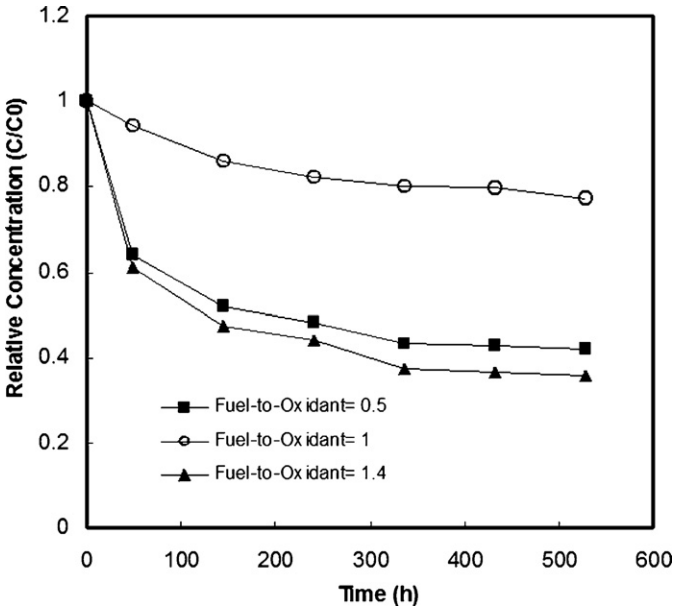

Fig. 8. Relative supernatant particle concentration of nanofluids with sedimentation time.

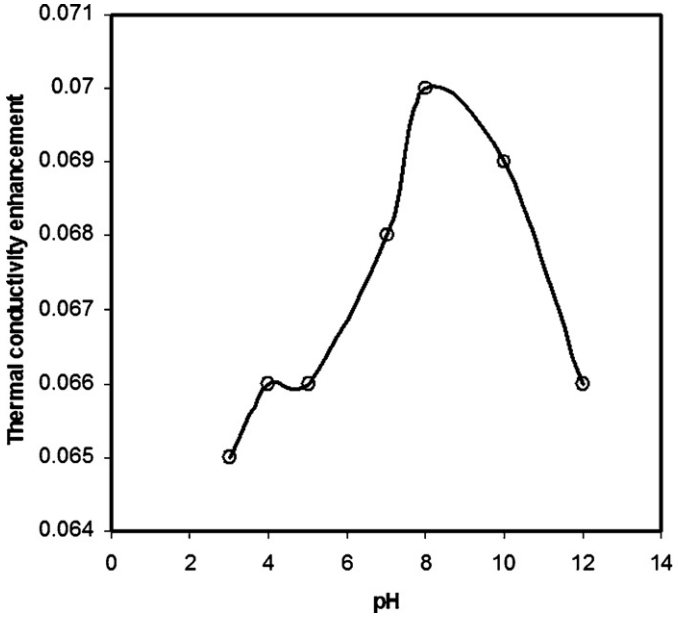

Fig. 10. Effect of pH on thermal conductivity of SN1.0 (0.024 wt%) nanofluid.

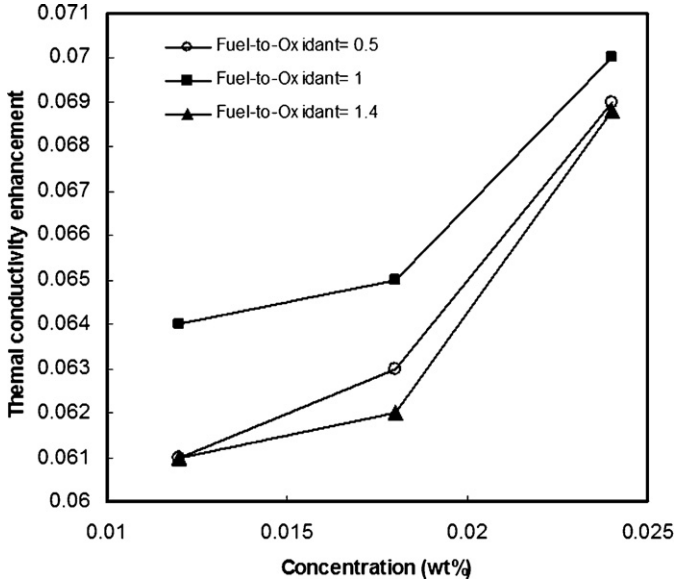

Fig. 11. Thermal conductivity enhancement of nanoparticles synthesized at various fuel-to-oxidant ratio suspensions as a function of solid weight fraction.

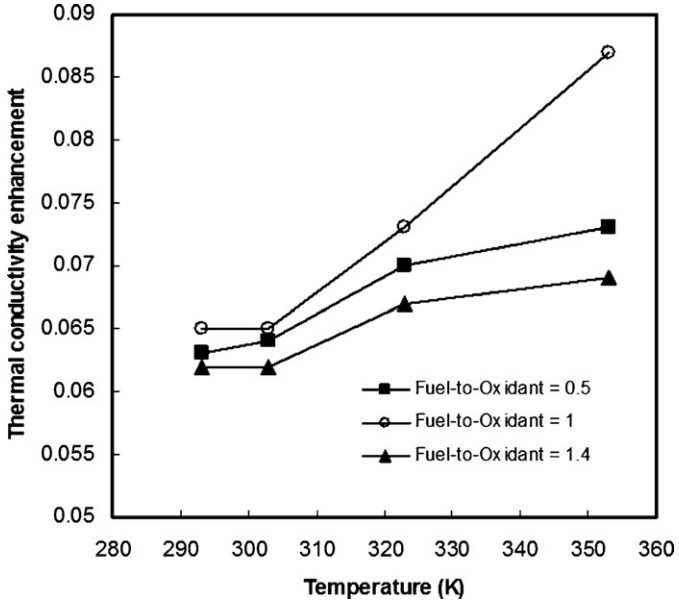

Fig. 12. Thermal conductivity enhancement of nanoparticles synthesized at various fuel-to-oxidant ratio suspensions as a function of temperature.

4. Conclusion

Stability of nanofluids of tin dioxide prepared by a novel combustion synthesis method at lean, stoichiometric and rich fuel conditions have been estimated by UV–vis analyses. Stability of nanofluids is strongly affected by the characteristic of suspended particles. The experimental results disclose that the nanofluid prepared by SnO_2 nanoparticles synthesized at $\Phi = 1.0$ (SN1.0) with higher surface area, lower aggregation ratio and thereby fine crystallite size is the most stable nanofluid.

Thermal-transport behavior of nanofluids is highly affected by the dispersion and stability of nanoparticles in a base fluid. Thermal conductivity enhancement of prepared nanofluids was measured using the transient hot-wire method. It was shown that thermal conductivity enhancement depends upon the pH value, nanoparticles concentration and temperature. The results also show there are more surface charges at around pH 8.0, at which the thermal conductivity is higher. The maximum thermal conductivity enhancement of up to 8.7% is observed for SN1.0 at 353 K.

References

[1] H.E. Patel, S.K. Das, T. Sundararajan, A. Sreekumaran Nair, B. George, T. Pradeep, Thermal conductivities of naked and monolayer protected metal nanoparticle based nanofluids: manifestation of anomalous enhancement and chemical effects, Appl. Phys. Lett. 83 (2003) 2931.
[2] W. Yu, U.S. Choi, The role of interfacial layers in the enhanced thermal conductivity of nanofluids: a renovated Maxwell model, J. Nanoparticle Res. 5 (2003) 167–171.
[3] S.U.S. Choi, Developments and Applications of Non-Newtonian Flows, vol. 231, ASME, New York, 1995, pp. 99–102.
[4] P. Keblinski, J.A. Eastman, D.G. Cahill, Nanofluids for thermal transport, Mater. Today 8 (2005) 36–44.
[5] Y. Hwang, J.K. Lee, C.H. Lee, Y.M. Jung, S.I. Cheong, C.G. Lee, B.C. Ku, S.P. Jang, Stability and thermal conductivity characteristics of nanofluids, Thermochim. Acta 455 (2007) 70–74.
[6] Y. Hwang, J.K. Lee, J.K. Lee, Y.M. Jeong, S.I. Cheong, Y.C. Ahn, S.H. Kim, Production and dispersion stability of nanoparticles in nanofluids, Powder Technol. 186 (2008) 145–153.
[7] S. Lee, S.U.S. Choi, S. Li, J.A. Eastman, Measuring thermal conductivity of fluids containing oxide nanoparticles, J. Heat Transf. 121 (1999) 280–289.
[8] P. Keblinski, S. Phillpot, S. Choi, J. Eastman, Mechanisms of heat flow in suspensions of nano-sized particles (nanofluids), Int. J. Heat Mass Transf. 45 (2002) 855–863.
[9] J. Buongiorno, Convective transport in nanofluids, J. Heat Transf. 128 (2006) 240.
[10] H. Zhu, Y. Lin, Y. Yin, A novel one-step chemical method for preparation of copper nanofluids, J. Colloid Interface Sci. 227 (2004) 100–103.
[11] X. Wang, X. Xu, S.U.S. Choi, Thermal conductivity of nanoparticle–fluid mixture, J. Thermophys. Heat Transf. 13 (1999) 474–480.
[12] G. Korotchenkov, V. Brynzari, S. Dmitriev, Electrical behavior of SnO_2 thin films in humid atmosphere, Sens. Actuators B 54 (1999) 197.
[13] Y. Zhao, Z. Feng, Y. Liang, SnO_2 gas sensor films deposited by pulsed laser ablation, Sens. Actuators B 56 (1999) 224.
[14] L. Bruno, C. Pijolat, R. Lalauze, Tin dioxide thin-film gas sensor prepared by chemical vapor deposition: influence of grain size and thickness on the electrical properties, Sens. Actuators B 18 (1994) 195–199.
[15] S.I. Rembeza, E.S. Rembeza, T.V. Svistova, O.I. Borsiakova, Electrical resistivity and gas response mechanisms of nanocrystalline SnO_2 films in a wide temperature range, Phys. Status Solidi A 179 (2000) 147.
[16] C. Wang, Y. Hu, Y. Qian, G. Zhao, A novel method to prepare nanocrystalline SnO_2, Nanostruct. Mater. 7 (1996) 421.
[17] S. Habibzadeh, Y. Mortazavi, A.A. Khodadadi, Novel microwave-induced combustion synthesis of SnO_2 nanoparticles for selective sensing of CO using tin chloride, J. NanoSci. Nanotechnol., in press.
[18] A.S. Mukasyan, P. Epstein, P. Dinka, Solution combustion synthesis of nanomaterials, Proc. Combust. Inst. 31 (2007) 1789.
[19] T. Mimani, K.C. Patil, Solution combustion synthesis of nanoscale oxides and their composites, Mater. Phys. Mech. 4 (2001) 134.
[20] R.D. Purohit, B.P. Sharma, K.T. Pillai, A.K. Tyagi, Ultrafine ceria powders via glycine–nitrate combustion, Mater. Res. Bull. 36 (2001) 2711.
[21] P. Erri, P. Pranda, A. Varma, Oxidizer–fuel interactions in aqueous combustion synthesis. 1. Iron (III) nitrate-model fuels, Ind. Eng. Chem. Res. 43 (2004) 3092.
[22] K.C. Patil, S.T. Aruna, T. Mimani, Combustion synthesis—an update, Curr. Opin. Solid State Mater. Sci. 6 (2002) 507.
[23] L. Fraigi, D.G. Lamas, N.E. Walsoe de Reca, Novel method to prepare nanocrystalline SnO_2 powders by a gel-combustion process, NanoStruct. Mater. 11 (1999) 311.
[24] G. Neri, A. Bonavita, G. Micali, N. Donato, F.A. Deorsola, P. Mossino, I. Amato, B. De Benedetti, Ethanol sensors based on Pt-doped tin oxide nanopowders synthesized by gel-combustion, Sens. Actuators B 117 (2006) 196.
[25] V. Srider, Microwave radiation as a catalyst for chemical reactions, Curr. Sci. 74 (1998) 446.
[26] S.M.S. Murshed, K.C. Leong, C. Yang, Investigations of thermal conductivity and viscosity of nanofluids, Int. J. Therm. Sci. 47 (2008) 560–568.
[27] S.M.S. Murshed, K.C. Leong, C. Yang, Enhanced thermal conductivity of TiO_2–water based nanofluids, Int. J. Therm. Sci. 44 (2005) 367–373.
[28] J.A. Eastman, S.U.S. Choi, S. Li, W. Yu, L.J. Thompson, Anomalously increased effective thermal conductivities of ethylene glycolbased nanofluids containing copper nanoparticles, Appl. Phys. Lett. 78 (2001) 718–720.
[29] Y.J. Hwang, Y.C. Ahn, H.S. Shin, C.G. Lee, G.T. Kim, H.S. Park, J.K. Lee, Investigation on characteristics of thermal conductivity enhancement of nanofluids, Curr. Appl. Phys. 6 (2006) 1068–1071.
[30] J.H. Lee, K.S. Hwang, S.P. Jang, B.H. Lee, J.H. Kim, S.U.S. Choi, C.J. Choi, Effective viscosities and thermal conductivities of aqueous nanofluids containing low volume concentrations of Al_2O_3 nanoparticles, Int. J. Heat Mass Transf. 51 (2008) 2651–2656.
[31] L. Chen, H. Xi, Y. Li, W. Yu, Applications of cationic gemini surfactant in preparing multi-walled carbon nanotube contained nanofluids, Colloids Surf. A 330 (2008) 176–179.

[32] X.F. Li, D.S. Zhu, X.J. Wang, N. Wang, J.W. Gao, H. Li, Thermal conductivity enhancement dependent pH and chemical surfactant for Cu–H_2O nanofluids, Thermochim. Acta 469 (2008) 98–103.
[33] Z. Chen, Y.W. Yan, J.-M. Liu, et al., Microwave induced solution combustion synthesis of nano-sized phosphors, J. Alloys Compd. 473 (2009) L13–L16.
[34] Y.P. Fu, C.H. Lin, Microwave-induced combustion synthesis of $Li_{0.5}Fe_{2.5-x}Mg_xO_4$ powder and their characterization, J. Appl. Phys. 105 (2009), 07A505.
[35] S.R. Jain, K.C. Adiga, V.R. Pai Verneker, A new approach to thermochemical calculations of condensed fuel-oxidizer mixtures, Combust. Flame 40 (1981) 71–79.
[36] Y. Nagasaka, A. Nagashima, Absolute measurement of the thermal conductivity of electrically conducting liquids by the transient hotwire method, J. Phys., E 14 (1981) 1435–1440.
[37] L. Jiang, L. Gao, J. Sun, Production of aqueous colloidal dispersions of carbon nanotubes, J. Colloid Interface Sci. 260 (2003) 89–94.
[38] W.B. Russel, D.A. Saville, W.R. Schowwalter, Colloidal Suspensions, Cambridge University Press, Cambridge, 1989.
[39] M. Elimelech, J. Gregory, X. Jia, R.A. Williams, Particle Deposition and Aggregation: Measurement, Modeling and Simulation, Butterworths, Oxford, 1995.
[40] F.Q. Tang, X.X. Huang, Y.F. Zhang, J.K. Guo, Effect of dispersants on surface chemical properties of nano-zirconia suspensions, Ceram. Int. 26 (2000) 93–97.